J. Phys.: Condens. Matter 1 (1989) 7013–7020. Printed in the UK

Fermi surface and electrical resistivity of Cu–Pt alloys: a relativistic calculation

J Banhart†, P Weinberger‡ and J Voitländer†

† Institut für Physikalische Chemie, Universität München, Sophienstrasse 11, 8000 München 2, Federal Republic of Germany

‡ Institut für Technische Elektrochemie, Technische Universität Wien, Getreidemarkt 9, 1060 Wien, Austria

Received 25 April 1989, in final form 5 June 1989

Abstract. The Fermi surface geometry and the electrical resistivity have been calculated in the framework of the fully relativistic Korringa–Kohn–Rostoker coherent potential approximation (KKR CPA) for a series of Cu–Pt alloys. Bloch spectral functions have been used to determine the position of the Fermi surface in various directions in k-space and to discuss band structure like behaviour. This information served as input data for the electrical resistivity calculation by means of a formula derived from the Boltzmann equation. The calculated electrical resistivities and the experimental data agree with each other very well.

1. Introduction

The coherent potential approximation (CPA) is a powerful and reliable tool in studying the electronic structure of substitutionally disordered alloys. In particular, the KKR version of the CPA dealing with muffin-tin Hamiltonians yields good results for a wide range of alloys. The relativistic extension of the KKR CPA has lifted the restriction of the CPA to light elements and allows treatment of alloys containing heavy elements like platinum.

In this paper, we present fully relativistic KKR CPA calculations for Cu–Pt alloys. These are particularly interesting, because a disordered FCC phase exists over the whole range of composition (metastable phase), and additionally two different ordered phases (Hansen and Anderko 1958) in the concentration range 10 at.% $< x_{Cu} <$ 71 at.% ($L1_1$-type) and 71 at.% $< x_{Cu} <$ 90 at.% ($L1_2$-type). Both disordered and ordered phases can be prepared by special thermal and mechanical treatment (Banhart *et al* 1988b, 1989b).

The CPA can only account for the disordered state. The case of short-range order (SRO) or long-range order (LRO) has to be investigated with different methods. The embedded cluster method (ECM) based on the CPA was successfully applied to the Cu–Pt system, in order to interpret alloy properties related to the Fermi energy (Banhart *et al* 1988a, 1988c) and the complete valence energy regime (Banhart *et al* 1989b) in previous publications. These papers show that the methods based on the CPA produce good and reliable results. In this paper, we discuss k-space-related properties for the disordered state, such as the Fermi surface and the electrical resistivity.

0953-8984/89/397013+08$02.50

2. Theory

The relativistic CPA equations (Staunton *et al* 1980) were solved for an angular momentum up to $l_{max} = 2$. The Brillouin-zone integration of the KKR matrix was carried out using 21 special directions (Fehlner and Vosko 1976) and between 30 and 900 k-points per direction. For the iterative solution of the CPA equations, the application of the Mills iteration scheme to the KKR CPA (Ginatempo and Staunton 1988) was used. The Fermi energy was determined by use of Lloyd's formula for the integrated density of states (Staunton *et al* 1980). All calculations were based on site potentials according to the Mattheiss description and on experimental lattice constants (Linde 1937). Once the KKR CPA equations had been solved, relativistic Bloch spectral functions were calculated (Weinberger *et al* 1982). Varying $\boldsymbol{k}$ for fixed energy E, the Fermi surface and the electrical resistivity can be determined. Varying E for fixed $\boldsymbol{k}$, alloy properties related to the band structure can be discussed.

The electrical resistivity can be calculated using a formula derived from Boltzmann's equation (Rossiter 1987). Within this approach, the complicated full Boltzmann equation is first transformed to the linearised Boltzmann equation on the assumption of microreversibility and only small deviations of the electronic distribution function from the equilibrium distribution function (Fermi distribution). Then exponential relaxation of the non-equilibrium distribution into equilibrium is applied to the scattering term (relaxation time approximation). Note that this approximation neglects the 'scattering-in' terms in the Boltzmann equation. Also the existence of electronic states with well defined band indices n and $\boldsymbol{k}$ is required within this approximation, which implies the existence of a dispersion relation for the electrons. The resulting simplified equation can be used to calculate the proportionality between the electrical field $\boldsymbol{E}$ and the current density $\boldsymbol{j}$ (electrical conductivity tensor). For cubic crystal symmetry there is only one scalar component of the conductivity σ, which is the inverse of the resistivity ρ (Rossiter 1987):

$$\sigma = \frac{1}{\rho} = \frac{2}{3}\frac{e^2}{\hbar}\frac{1}{(2\pi)^3}\iint_{FS} l(\boldsymbol{k}_F)\,\mathrm{d}S(\boldsymbol{k}_F) \tag{1}$$

In equation (1) $l(\boldsymbol{k}_F)$ is the electronic quasi-particle mean free path at the Fermi energy. Figure 1 shows how this quantity is determined using Bloch spectral functions. The

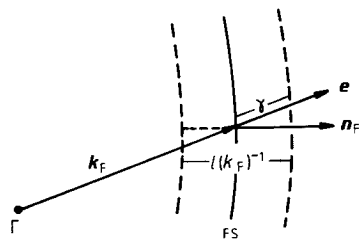

Figure 1. Schematical representation of the various quantities involved in the calculation of $l(\boldsymbol{k}_F)$. The broken curves indicate the halfwidth of the Fermi surface (FS) determined from Bloch spectral functions in the direction $\boldsymbol{e}$. $\boldsymbol{n}_F$ is the unit vector orthogonal to the FS.

Bloch spectral function in the special direction $\boldsymbol{e}$, $A_B(k\boldsymbol{e}, E_F)$, is approximated by a Lorentzian $a + bk + c/[(k - k_F)^2 + \gamma^2]$. The $\boldsymbol{k}_F$ localises the Fermi surface position and γ determines the half width of the smeared surface in this particular direction. Now $l(\boldsymbol{k}_F)$ is the inverse of the width along the normal unit vector onto the Fermi surface $\boldsymbol{n}_F$ so $2(\gamma \boldsymbol{e}) \cdot \boldsymbol{n}_F = l(\boldsymbol{k}_F)^{-1}$. Using this formula, $l(\boldsymbol{k}_F)$ can be determined from the Bloch spectral functions (Butler and Stocks 1984).

The surface integral in equation (1) was calculated using 136 directions in the irreducible wedge of the FCC Brillouin zone. In some cases, the directions cut through two or three sheets of the Fermi surface so that two or three Lorentzians had to be used to fit the Bloch spectral functions.

3. Results and discussion

3.1. Band structure

For a first survey of the location of the energy bands in the Cu–Pt alloys, we calculated the band structure of a fictitious FCC lattice consisting of only Cu or Pt atoms with the potentials and the lattice constant of a $Cu_{60}Pt_{40}$ alloy. The resulting band structure is shown in figure 2 for the Γ–X direction. The Fermi energy of the alloy as calculated within the CPA framework cuts through the Pt d band while it is well above the Cu d bands. This indicates a quite different behaviour of the two components' densities of states at this energy (Banhart 1989).

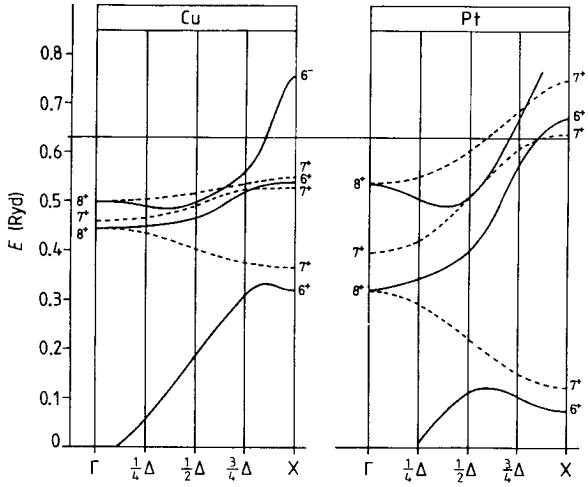

Figure 2. Band structure of a fictitious FCC lattice occupied by either the Cu (left-hand side) or Pt (right-hand side) potentials of $Cu_{60}Pt_{40}$ (with the lattice constant of the alloy). Full curve: Δ_6-symmetry, broken curve: Δ_7-symmetry.

3.2. Constant-k Bloch spectral functions

The band structures in figure 2 serve well in interpreting the Bloch spectral functions at the Γ point shown in figure 3 for two alloys. For the Pt-rich alloy $Cu_{15}Pt_{85}$ we see three distinct peaks. They can easily be related to the Γ_{8+},Γ_{7+},Γ_{8+} states of Pt in figure 2. The same behaviour can be seen for the Cu-rich alloy $Cu_{85}Pt_{15}$ where also three peaks occur which can be identified as the analogous states of Cu at the Γ point.

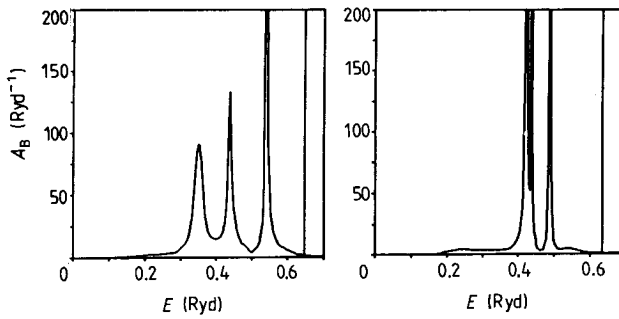

Figure 3. Bloch spectral functions A_B for $\boldsymbol{k} = (0,0,0)$. Left: $Cu_{15}Pt_{85}$, right: $Cu_{85}Pt_{15}$. Vertical line: Fermi energy.

While the Bloch spectral functions do not really define bands in the sense of a well defined dispersion relation, they nevertheless seem to be well localised and fairly narrow, and can therefore be interpreted as lifetime broadened, smeared quasi-bands.

3.3. Constant-E Bloch spectral functions

An observation similar to that in the preceding paragraph can be made for constant-energy Bloch spectral functions at $E = E_F$ and varying $\boldsymbol{k}$. Figure 4 shows two examples with compositions as in figure 3. Again rather sharp and localised Lorentzian peaks occur. We therefore tried to fit Lorentzian model functions to the set of calculated values of the Bloch spectral function (triangles in figure 4). Apparently, the fit can be done very well so that a definite position and width can be assigned to the Bloch spectral function. Again we can argue that—especially in the Cu-rich alloys—a kind of quasi-band structure is defined. This enables us to define Fermi surface sheets and to make use of the Boltzmann equation for the calculation of the electrical resistivity. The position of the maxima of the Bloch spectral functions in figure 4 is the position of the Fermi surface sheet in this specific direction. By evaluating Bloch spectral functions in this way for a set of special directions which span two planes in the first Brillouin zone we arrive at a representation of the Fermi surface as Fermi surface cuts.

These cuts are shown in figure 5. For comparison, the Fermi surfaces of the pure metals Pt (Andersen 1970) and Cu (MacDonald *et al* 1982) have been included in this figure. Pure Cu has the well known Fermi surface with the wide neck in the [111] direction (L point). When Pt is alloyed to Cu, the Fermi surface begins to shrink due to the reduction of the number of electrons. This occurs everywhere on the surface and especially in the L and K directions. As a consequence, the [111] neck becomes narrower, and the Fermi surface in the [110] direction (K point) gradually looses its curvature and flattens out. Additionally, the width of the Fermi surface increases with increasing Pt content. In $Cu_{60}Pt_{40}$, a second sheet of the Fermi surface can be seen developing around the X point and growing towards the W and K points and towards the U and L points with increasing Pt concentration. In the equiatomic alloy, the largest smearing of the inner sheet of the surface occurs. For even higher Pt concentrations this sheet starts to narrow again. In $Cu_{30}Pt_{70}$, the [111] neck has disappeared, and the corresponding sheet moves inwards for even higher Pt concentrations. For 15 at.% Cu, the second sheet of the Fermi surface has reached the K and L points and a third sheet develops between the L and U points and around the X point. For 5 at.% Cu the situation is very much like that in pure Pt. The inner sheet of the Fermi surface is already very narrow, the outer sheets resemble the corresponding sheets in pure Pt.

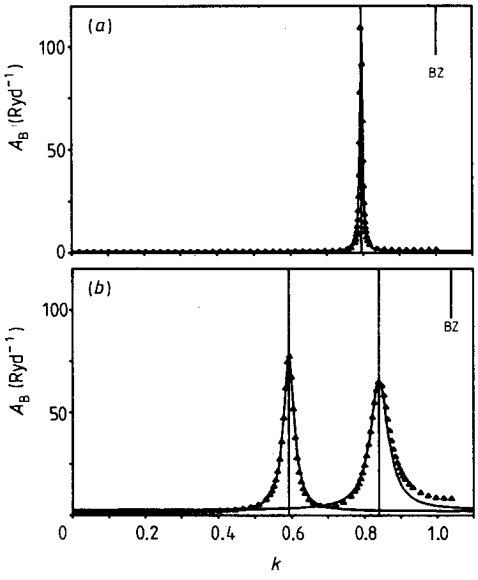

Figure 4. Bloch spectral functions A_B for $E = E_F$ in a special direction $\boldsymbol{e}$. (*a*): $Cu_{85}Pt_{15}$, $\boldsymbol{e} = (0.073, 0, 1)$; (*b*): $Cu_{15}Pt_{85}$, $\boldsymbol{e} = (0.271, -0.03, 0.962)$. The triangles are the calculated values. A Lorentzian function is fitted to each peak by a least square approximation shown as a full curve. The maximum positions and Brillouin zone positions are indicated as vertical lines.

Local-order diffuse electron scattering experiments can reveal Fermi surface effects under certain conditions. It has been shown (Moss 1969) that in the directions where the Fermi surface is narrow and has a low curvature, multiply split scattering spots occur, the separation of which is related to the length of the Fermi vector in the specific direction. Looking at figure 5 it seems probable that the effect may occur in the K direction [110] for Cu-rich alloys. Indeed the effect has been observed for a number of Cu–Pt alloys (Oshima and Watanabe 1973, Chevalier and Stobbs 1979). In figure 6 the Fermi vectors $\boldsymbol{k}_{110}$ in the [110] direction derived from the experimental data are compared with the calculated ones. The length of $\boldsymbol{k}_{110}$ increases monotonously with Cu concentration both for the theoretical and experimental values. However, the experimental values are larger by about 5 to 7% than our calculated ones. This deviation is not very large, so we state that the agreement between theory and experiment is satisfactory.

An interesting fact about the Fermi surfaces is that for all compositions the various sheets are well defined. This is especially true for the first sheet which contributes predominantly to the electrical conductivity. Thus, the evaluation of the surface integral in equation (1) makes sense, and the Boltzmann equation can be expected to yield good results for the electrical resistivity.

3.4. Electrical resistivity

Since there are various sheets of the Fermi surface in Cu–Pt alloys, the integral in equation (1) can be written as a sum of integrals, each one referring to one particular sheet. Therefore, the electrical conductivity can be split into a sum of contributions one corresponding to each one of the three sheets. Table 1 lists the contributions for the various compositions and sheets. For all alloys, the first sheet contributes most to the electrical conductivity. This is due to the fact that the first sheet is narrower than the other sheets. This makes the quantity $l(\boldsymbol{k}_F)$ in equation (1) large. The second sheet is important only in the Pt-rich alloys, contributing 41% to the conductivity for $Cu_{30}Pt_{70}$. The third sheet is of minor importance. The results for the electrical

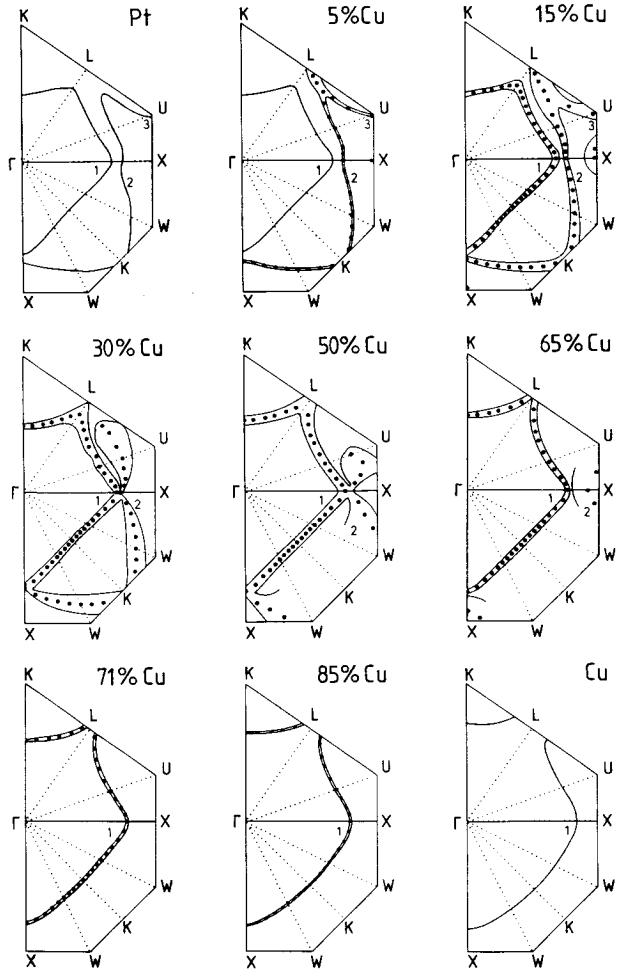

Figure 5. Fermi surface cuts in the planes Γ–X–U–L–K and Γ–X–W–K. The pure metal Fermi surfaces have also been included (Pt (Andersen 1970), Cu (MacDonald *et al* 1982)). Dots indicate maxima of the Bloch spectral functions, the contour lines indicate the halfwidth of the peaks The numbering refers to the numbers of the Fermi surface sheets in table 1.

(residual) resistivity are shown in figure 7, which also includes experimental values (Linde 1937).

Johansson and Linde published two sets of values for the disordered state (Johansson and Linde 1927, Linde 1937)), one referring to cold rolled alloys, the other one to alloys quenched from 900°C. Both values differ from each other. However, while being quenched from 900°C the alloys tend to order, because the atomic mobility is very high at this temperature (see the experimental work on Cu–Pt by Banhart *et al* (1988b, 1989a). Therefore we consider the cold rolled state to be closest to the disordered state and compare our theoretical values with the experimental values of that state. For an otherwise perfect lattice only the contribution of disorder to the resistivity is of interest. Therefore the theoretical values for pure metals are zero by

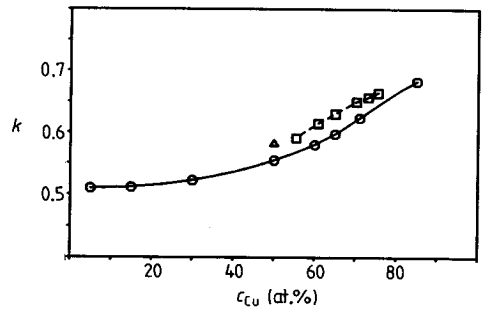

Figure 6. Length of k-vectors in the [110] direction, in terms of the distance Γ–X. Circles: calculated values; squares: values derived from experimental data (Oshima and Watanabe 1973); triangle: value derived from experimental data (Chevalier and Stobbs 1979).

Table 1. Calculated electrical conductivity of Cu–Pt. For each sheet the calculated value (units: 10^6 S m^{-1}) and its relative contribution to the sum (in %) is given.

at.% Cu	First sheet		Second sheet		Third sheet		Sum
0	∞	—	∞	—	∞	—	∞
5	5.03	58	3.05	35	0.67	7	8.76
15	1.52	57	1.04	39	0.12	4	2.68
30	0.81	59	0.56	41	0	0	1.37
50	0.90	87	0.13	13	0	0	1.03
60	1.23	95	0.07	5	0	0	1.30
65	1.61	98	0.03	2	0	0	1.64
71	2.47	100	0	0	0	0	2.47
85	5.69	100	0	0	0	0	5.69
100	∞	100	0	0	0	0	∞

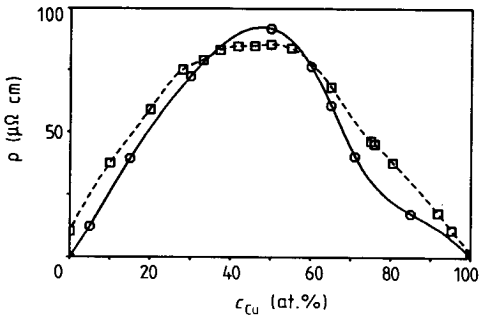

Figure 7. Electrical resistivity of Cu–Pt alloys. Circles: calculated values for the residual resistivity due to disorder (zero for the pure components by definition); squares: experimental values for the resistivity of a cold-rolled Cu–Pt specimen at 18°C (Linde 1937). The individual points have been joined for clearer representation.

definition while the experimental values reflect other contributions to the resistivity like impurity scattering, lattice defects and thermal vibrations and have in general a non-zero value. These contributions are high (10 $\mu\Omega$ cm) especially for pure Pt. In the range between 0 and 30 at.% Cu all theoretical values are lower than the experimental ones by about 10 $\mu\Omega$ cm. So one could speculate that this offset is caused by an extra non-disorder contribution to the experimental values in the Pt-rich alloys. The

maximum of the experimental resistivity around 50 at.% Cu is reproduced quite well by the theoretical values. On the copper rich side some disagreement between theoretical and experimental resistivities occurs, which is most significant around 80 at.% Cu. As the experimental value for Cu is very small, an explanation for the deviations between theoretical and experimental values similar to that for the Pt-rich alloys is not possible. The deviations could be linked to the use of potentials not obtained self-consistently in our calculations, or to a failure of the approximations made for the Boltzmann equation.

4. Summary

The description of k-space-related properties of Cu–Pt alloys by means of Bloch spectral functions has been shown to yield a picture of quasi-bands, quasi-states and quasi-Fermi surfaces. The application of the Boltzmann equation to the electrical resistivity results in values which are in good agreement with experimental values, in particular in view of the fact that no adjustable parameters enter the calculations. The question whether certain deviations from experiment have to be explained as an effect of the lack of self-consistency in the potential construction cannot be answered definitely here. However, the application of the same potentials in other calculations (Banhart *et al* 1988a, c, 1989b, Banhart 1989) has shown that the Mattheiss description works rather well for the case of Cu–Pt. So perhaps the assumptions inherent in equation (1) limit the accuracy. Application of the more advanced Kubo formula to the alloy system (Butler 1985) could help to clarify this question.

Acknowledgment

The grant by the Austrian Ministry of Science (G.Z.49.554/3-24/87) is thankfully acknowledged by P Weinberger.

References

Andersen O K 1970 *Phys. Rev.* B **2** 883
Banhart J 1989 *Thesis* Universität München
Banhart J, Pfeiler W and Voitländer J 1988b *Phys. Rev.* B **37** 6027
—— 1989b *Alloy Phase Stability* NATO ASI Series E, vol 163 (Dordrecht: Kluwer) p 131
Banhart J, Weinberger P, Ebert H and Voitländer J 1988a *Solid State Commun.* **65** 693
—— 1988c *J. Appl. Phys.* **63** 4130
Banhart J, Weinberger P and Voitländer J 1989c to be published
Butler W H 1985 *Phys. Rev.* B **31** 3260
Butler W H and Stocks G M 1984 *Phys. Rev.* B **29** 4217
Chevalier J P and Stobbs W H 1979 *Acta Metall.* **27** 285
Fehlner W H and Vosko S H 1976 *Can. J. Phys.* **54** 2159
Ginatempo B and Staunton J B 1988 *J. Phys. F: Metal Phys.* **18** 1827
Hansen M and Anderko K 1958 *Constitution of Binary Alloys* (New York: McGraw Hill)
Johansson C H and Linde J O 1927 *Ann. Phys., Lpz* **82** 449
Linde J O 1937 *Ann. Phys., Lpz* **30** 151
MacDonald A H, Daams J M, Vosko S H and Koelling D D 1982 *Phys. Rev.* **25** 713
Moss S C 1969 *Phys. Rev. Lett.* **22** 1108
Oshima K and Watanabe D 1973 *Acta Crystallogr.* A **29** 520
Rossiter P L 1987 *The Electrical Resistivity of Metals and Alloys* (Cambridge: CUP)
Staunton J B, Gyorffy B L and Weinberger P 1980 *J. Phys. F: Metal Phys.* **10** 2665
Weinberger P, Staunton J B and Gyorffy B L 1982 *J. Phys. F: Metal Phys.* **12** 2229